

Universiteit Twente.

Faculty of Science and Technology

# **Oleophobic surfaces by PDMS molding**

From simple techniques to advanced surfaces

**A thesis submitted for the degree of**

**Bachelor of Science**

**presented by Pim Bullée**

p.a.bullee@student.utwente.nl

May, 2012

# Contents

<b>1</b>	<b>Introduction</b>	<b>5</b>
<b>2</b>	<b>Theoretical Background</b>	<b>8</b>
2.1	Contact Angle Hysteresis . . . . .	8
2.2	Wenzel and Cassie Baxter . . . . .	9
2.3	Bouncing droplet . . . . .	12
<b>3</b>	<b>Experimental</b>	<b>16</b>
3.1	Sample preparation . . . . .	16
3.2	Experimental setup . . . . .	19
3.3	Data processing . . . . .	20
<b>4</b>	<b>Results and Discussion</b>	<b>21</b>
4.1	Hysteresis . . . . .	21
4.2	Bouncing Droplet . . . . .	24
<b>5</b>	<b>Conclusions and Recommendations</b>	<b>29</b>
<b>A</b>	<b>Remaining Pictures and Graphs</b>	<b>30</b>

## Preface

This report is the result of my bachelor assignment for Advanced Technology. From November 2011 till the end of May 2012 I participated in a research on superhydrophobic and oleophobic surfaces. This research is a collaboration between the Soft matter, Fluidics and Interfaces group from the University of Twente and the spinoff company Lightmotif.

I would like to thank Rob Lammertink, head of the Sfi group, for the opportunity to participate in this research. Also I would like to thank Gor Manukyan, who started as my daily supervisor and showed me around in the lab. Amy Peichun was of great help with the last part on bouncing droplets. Ineke Punt helped me understand some crucial parts of the research and provided lots of SEM images. Ruud van Damme agreed to be the external member of the Bachelor committee, which I really appreciate since he is my mentor and in my opinion a very good teacher. Last but not least I would like to thank all the members and students of the Sfi group for the great time I had during this assignment.

## Abstract

A new production method for superhydrophobic and oleophobic surfaces is being revised using PDMS molding. This relatively cheap method enables the low cost production of these surfaces, giving access to a new variety of applications. Surface structures with differing geometries were tested on oleophobic properties using contact angle hysteresis measurements and the observation of impinging droplets. The majority of the experiments were performed using ethylene glycol, featuring a lower surface tension and a higher viscosity than water. This showed good results with contact angle hysteresis below  $5^\circ$  and fully rebounding droplets from falling heights up to  $12.3\text{ mm}$ .

# 1 Introduction

Surfaces which show a strong water repellent behavior are of large interest for a variety of applications. Think of anti-icing on airplane wings and car windows, self cleaning clothes and surfaces, but also on the terrain of microfluidics these surfaces can offer advantages. This is an area of research which is very popular and still growing [14] [23]. Superhydrophobic materials have a water contact angle larger than  $150^\circ$ , which enables water droplets to roll off the surface easily. This contact angle is measured through the liquid, between the surface and the liquid-vapor interfaces, as also can be seen in Figure 2. A well chosen surface morphology can turn a hydrophilic surface (which attracts water) into a superhydrophobic surface [5]. The high surface tension and polarity of water make superhydrophobic surfaces readily achievable. For fluids with a lower surface tension, such as oils, this is more difficult, since these fluids prefer a wetting state; contact angles below  $90^\circ$  [23].

The concept of surface tension is most easily made clear using Figure 1. In the bulk of a fluid, a single molecule is surrounded by other molecules. These molecules exert an attracting force on this single molecule, known as cohesion. The net resultant force on the molecule is zero, since it is surrounded by equal molecules. At the surface, the molecule is not surrounded anymore, resulting in a net cohesive force called surface tension. It is a form of potential energy proportional to the surface area of the liquid. Since nature strives for a minimum of potential energy, liquids will attempt to minimize their surface area. This explains why bubbles and drops of liquid in air are spherical and also why fluids with a lower surface tension prefer a wetting state [6].

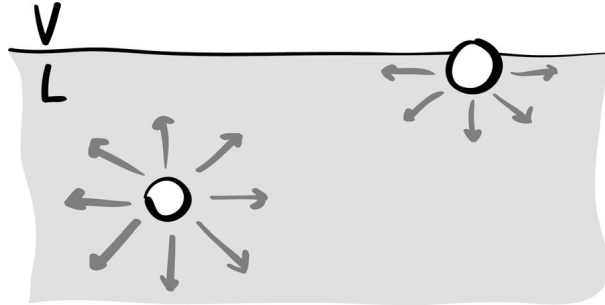


Figure 1: Molecules in the bulk of the fluid and at the surface. Note the difference between attractive forces from surrounding molecules. Figure adapted from [16].

The extent to which a liquid spreads over a surface (known as wettability) is determined by the chemistry and morphology of the surface, as well by the chemistry of the fluid. The influence of chemistry is shown by Young's equation, Eq. 1, as established in 1805 by Thomas Young in his paper on cohesion of fluids [29].

$$\cos \theta_Y = \frac{\gamma_{SV} - \gamma_{SL}}{\gamma_{LV}} \quad (1)$$

This equation relates the solid, liquid and vapor interfacial surface tensions,  $\gamma$ , to the

intrinsic contact angle,  $\theta_Y$ , also known as Young's angle. The balance between the three surface tensions determine the contact angle and the shape of the droplet. A visual representation of this is given in Figure 2, which is adapted from [16].

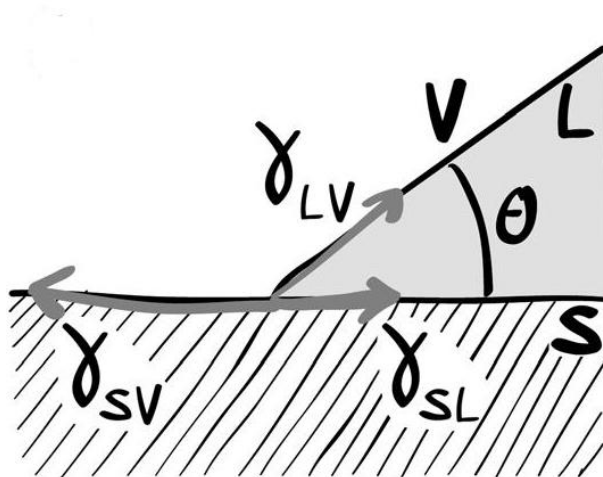


Figure 2: The triple interface between vapor, liquid and solid, formed by a liquid drop on a solid surface. Displayed is the left side of the droplet.

The influence of surface morphology on wettability is described by the Wenzel's and Cassie-Baxter's equations, respectively Eq. 5 and Eq. 8. They predict two metastable wetting states, as shown in Figure 3 named after their discoverers, in which the one with the lower contact angle is most stable [23]. In these equations  $r$  is the roughness ratio, the ratio between the true area of the surface and the area of the flat surface where it is placed upon. Thus, for a complete flat surface  $r = 1$  and  $r > 1$  for a rough surface.  $f_S$  and  $f_V$  are the fractions of fluid in contact with the solid and the vapor, respectively. The  $\theta_Y$ ,  $\theta_W$  and  $\theta_{CB}$  give the Young's contact angle (for a flat surface) and the contact angles for Wenzel and Cassie-Baxter state.

$$\cos \theta_W = r \cos \theta_Y \quad (2)$$

$$\cos \theta_{CB} = f_S \cos \theta_Y + f_S - 1 \quad (3)$$

When  $\theta_{CB}$  is set equal to  $\theta_W$ , this results in a critical Young's angle, above which the nonwetting Cassie-Baxter state is the more stable.

$$\cos \theta_{Y,c} = \frac{f_S - 1}{r - f_S} \quad (4)$$

This is an important result. Since  $f_s < 1 < r$ , this means that for the creation of an oleophobic surface (repellant to fluids with low surface tensions) using surface roughness, the contact angle for low surface tension fluids on the flat surface should already exceed  $90^\circ$ .

There are no known surfaces, which display this kind of behavior [23]. Therefore, the Wenzel state will always have the lowest potential energy and is therefore preferred by fluids with a low surface tension. To prevent the transition from Cassie-Baxter into Wenzel state, or to delay it as much as possible, the energy barrier between the two states should be as high as possible. Design criteria for oleophobic has already been a research topic over the past few years [10, 21, 25, 26]. Recently Savoy et al. have performed molecular simulations for oily fluids on rough surfaces, which predict the behavior of these fluids depending on surface design parameters [23].

The fabrication of superhydrophobic and oleophobic surfaces can be divided in two different manufacturing methods. The first one creates rough surfaces on hydrophobic materials. Examples are soft photolithography, sol-gel methods, upright carbon nanofibers or -tubes, electrospinning, oxidation of an aluminum surface or sandblasting. See also Lee et al. for more examples [14]. The second fabrication method alters a rough surface using materials with a low surface tension  $\gamma_{SV}$ , such as fluoroalkylsilane [14]. Usually these materials are applied using some sort of nano material distribution method or a coating method. This approaches the ‘lotus effect’ at best. This lotus effect is based on the leaves of the lotus, which features a micro-nano structure; a nanostructure on top of a microstructure [1, 20]. This makes the lotus leaves superhydrophobic. The result of this is that water drops falling on top of the leaves will roll off and on their way they will drag along dust and other dirt particles. The disadvantage of this method is that the distribution of the nanostructure is difficult to control, which makes the production of a reproducible surface challenging.

The fabrication method utilized in this study combines these two methods. A microstructure is molded in PDMS (polydimethylsiloxane). The PDMS we used displayed a flat surface water contact angle  $\theta_Y$  of about  $112^\circ$ , which is consistent with values from literature [17]. On this microstructure a coating of aluminum nanoparticles is applied which forms the nanostructure. Advantages of this method are the relatively low costs of production; the mold used for the PDMS can theoretically be reused endlessly. Also because it uses both fabrication methods, we expect to receive good results for both superhydrophobicity and oleophobicity.

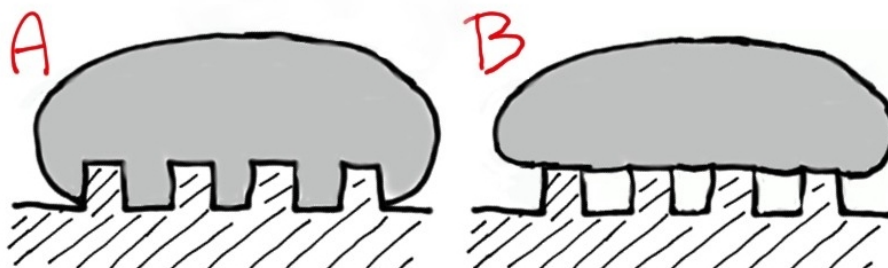


Figure 3: The metastable Wenzel (A) and Cassie-Baxter (B) states. The liquid in Wenzel state fills the structure, whilst the liquid Cassie-Baxter state lies on top of it.

## 2 Theoretical Background

### 2.1 Contact Angle Hysteresis

When a liquid droplet lies on top of a solid surface, it forms a spherical shape which is sectioned by the surface. The contact angle formed by the droplet is discrete and quite accurately measurable. However, the shape is not reproducible and the contact angle will usually vary by values up to  $20^\circ$  or even more [11]. Therefore, the equilibrium contact angle can not be used as a reference in determining surface properties.

When an amount of liquid is added to a droplet its volume will increase. At first the contact area with the solid substrate shall stay the same, so the contact angle has to increase. At a certain maximum value of contact angle the edge of the droplet will start to move outwards, since the droplet volume is still increasing. In a plot of contact angle versus time, this looks like a plateau. The contact angle at which this plateau occurs is called the advancing contact angle, usually denoted  $\theta_A$ . Vice versa, when liquid is removed from the droplet, its volume will decrease with decreasing contact angle. At some point the edge of the droplet will start to move inwards, whilst the contact angle stays constant. This angle is called the receding contact angle, denoted  $\theta_R$ , and also displayed by a plateau in the plot. The difference between the advancing and receding contact angle is termed hysteresis. Typical hysteresis curves look like the one in Figure 4.

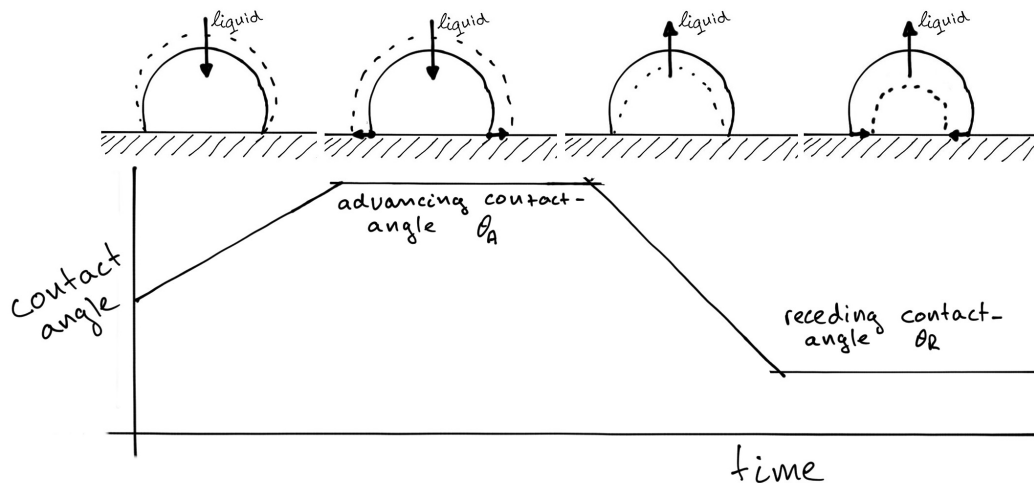


Figure 4: Contact angle hysteresis measurements graphically explained. The first two drawings show the addition of fluid resulting in an increasing contact angle, until the advancing contact angle  $\theta_A$  is reached. After this, the edge of the droplet starts to advance, as showed in the second drawing. When the added fluid is removed, first the contact angle decreases again, until the point that the edge of the droplet starts to recede and the receding contact angle  $\theta_R$  is reached. The difference between  $\theta_A$  and  $\theta_R$  is called contact angle hysteresis.

A droplet can display any contact angle between its advancing and receding contact angle. In order for a droplet to move on a tilted surface, it both has to advance the advancing contact angle (on the downhill side) and recede the receding contact angle (on the upper hill side). Therefore the amount of contact angle hysteresis  $\theta_A - \theta_R$  is a useful measurement in determining the hydrophobic properties of a surface. It gives an indication of the affinity between the solid and the liquid. Low contact angle hysteresis means a very hydrophobic surface and vice versa. On superhydrophobic surfaces ( $\theta > 150^\circ$ ), droplets will already start to move if the surface is only tilted a few degrees [11].

## 2.2 Wenzel and Cassie Baxter

These two theories were already introduced in Section 1, but will be explored further here. In particular the derivation of Wenzel's and Cassie-Baxter's equations will be concerned.

Young's equation (Eq. 1) is only valid for flat surfaces of a single type of material. It was pointed out by Wenzel that nano and micro structures on the surfaces modify the wetting properties [27]. Wenzel defined a surface roughness ratio factor  $r$ , the ratio between the true surface area of the structure and the flat surface where it is placed upon;  $r = A_{rough}/A_{flat}$ . Therefore  $r > 1$  for roughened surfaces and  $r = 1$  for a flat surface. This roughness factor can be substituted in Young's equation resulting in Wenzel's equation.

$$\cos \theta_W = r \cos \theta_Y = r(\gamma_{SV} - \gamma_{SL})/\gamma_{LV} \quad (5)$$

In this equation Young's angle  $\theta_Y$  is the contact angle of a flat surface, Wenzel's angle  $\theta_W$  is the contact angle of the roughened surface in the same conditions. Since  $\cos(90^\circ) = 0$ , this equation suggests that if  $\theta_Y < 90^\circ$  then  $\theta_W < \theta_Y$ . Also, if  $\theta_Y > 90^\circ$  then  $\theta_W > \theta_Y$ . This means that the addition of roughness to a flat surfaces enhances its hydrophobic or hydrophilic properties [5].

After Young's work, Cassie and Baxter discovered that for a substrate consisting of randomly distributed types of material, each material contributes to the net surface tension [7]. The contribution of each material is related to its material fraction presence on surface. For  $n$  different types of materials the sum of all fractions  $f_i$  equals 1. In the case of a flat surface, the net surface energies can be written in the form of Eq. 6.

$$\gamma_{Sx} = \sum_i^n f_i(\gamma_{i,Sx}) \quad (6)$$

In this equation  $x$  is either  $L$ , liquid or  $V$ , vapor, since the liquid-vapor interface is not influenced by the combined solid surface. When this is introduced with Wenzel's equation, Eq. 5, the resulting Cassie-Baxter equation also accounts for rough surfaces [5].

$$\cos \theta_{CB} = \sum_i^n r f_i \cos \theta_{i,Y} = \sum_i^n r f_i \frac{\gamma_{i,SV} - \gamma_{i,SL}}{\gamma_{LV}} \quad (7)$$

Certain rough surfaces structures can be shaped such that air pockets are trapped between the asperities. In this case it can be seen that the surface consists out of two

materials. One out of which the substrate is build and the other one is air, trapped in the surface between the asperities. An example of this is a solid flat surface, on which square posts are placed as seen in Figure 5. When a droplet is put on top of these structures, air is trapped between the surface, the posts and the liquid.

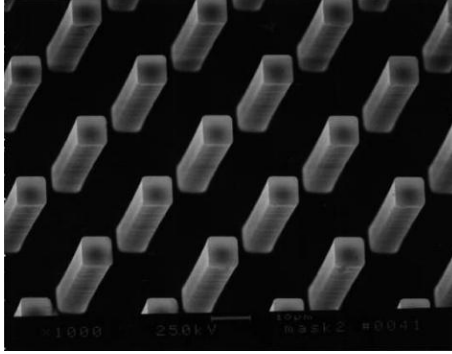


Figure 5: A flat surface on which  $8 \times 8 \times 40 \mu\text{m}$  square posts are placed. Figure adapted from [11].

Since liquid-vapor interfaces have a larger contact angle than liquid-solid interfaces, this can result in higher contact angles for the combined air-solid surface. For this surface morphology, the combined surface fractions of the solid and air (vapor) equal 1,  $f_S + f_V = 1$ . Substituted in Eq. 7 for  $n = 2$ , then  $f_1 = f_S$  and  $\cos \theta_{Y,1} = \cos \theta_Y$ . For the air pocket fraction  $f_2 = f_V$ ,  $r = 1$ , since the air has no roughness, and  $\cos \theta_{Y,2} = -1$ . The latter can be explained as that a liquid in a pure vaporous environment takes the shape of a perfect sphere. Therefore no wetting of the vapor occurs and the contact angle (vapor-liquid) everywhere on the sphere equals  $180^\circ$ . With these substitutions, the Cassie-Baxter equation (Eq. 7) results in the following equation.

$$\cos \theta_{CB} = r f_S \cos \theta_Y - f_V = r f_S \cos \theta_Y + f_S - 1 \quad (8)$$

Looking at the example in Figure 5, it is a reasonable assumption to state that a liquid lying on top of the square posts will only contact the top of the posts. In that case  $r$  equals one and can be left out of the equation.

As already displayed in Figure 3, in Wenzel state the liquid fills the structure and therefore increases its actual contact area by  $r$ , as also shown in Eq. 5. In Cassie-Baxter state, the liquid partly lies on top of the air pockets and thus decreases its actual solid-liquid contact area, resulting in a less adhesive interface. It is possible for a droplet to transit from Cassie-Baxter to Wenzel state. This has everything to do with the energy barrier between the states mentioned in Section 1. This barrier is for instance overcome by pressing the fluid into the structure. It is also possible for the states to coexist in the same droplet. Also droplet size is important for which state to be expected. Small droplets with high curvature are more likely to adept a Wenzel state than larger ones.

As is stated above and directly from Eq. 5, Wenzel's model only enhances the hydrophobic or hydrophilic surface properties. Cassie-Baxter's model also enables the pos-

sibility of evolution from below  $90^\circ$  flat surface Young's contact angles towards Cassie-Baxter angles higher than  $90^\circ$ . This means that hydrophilic flat surfaces can be made hydrophobic using a well chosen surface morphology. This is graphically displayed in Figure 6 where Wenzel's and Cassie-Baxter's equations are plotted as a function of Young's angle. Interesting to note is that a hydrophobic surface ( $\theta_Y > 90^\circ$ ) cannot be made hydrophilic using Cassie-Baxter's model. Figure 7 shows that for hydrophobic surfaces the modification of the roughness factor  $r$  and the fraction of solid in the surface  $f_s$  will not lead to a decrease of the Cassie-Baxter angle to values lower than  $90^\circ$ , if Young's contact angles initially already where larger then  $90^\circ$  [5].

The most important conclusion however was already drawn in Section 1, were an expression for the critical Young's was derived, repeated below in Eq 9.

$$\cos \theta_{Y,c} = \frac{f_s - 1}{r - f_s} \quad (9)$$

This equation showed that for the creation of oleophobic surfaces, the contact angle for low surface tension fluids on the flat surface should exceed  $90^\circ$ , since  $f_s < 1 < r$ . There are however no materials known that display that kind of behavior. Therefore it is only possible to delay the transition of Cassie-Baxter state into Wenzel state as long as possible. This is not necessarily discouraging, since Savoy et al. showed that droplets which display some hydrophobic properties on the flat surface, can maintain the Cassie-Baxter state for thousands of hours for well chosen surface morphologies. Droplets that show a more hydrophilic behavior can maintain their Cassie-Baxter state less then an hour [23]. Practically speaking however, for most applications a transition time in the order of hours would give more then enough time to remove the droplets from their surface before transitioning.

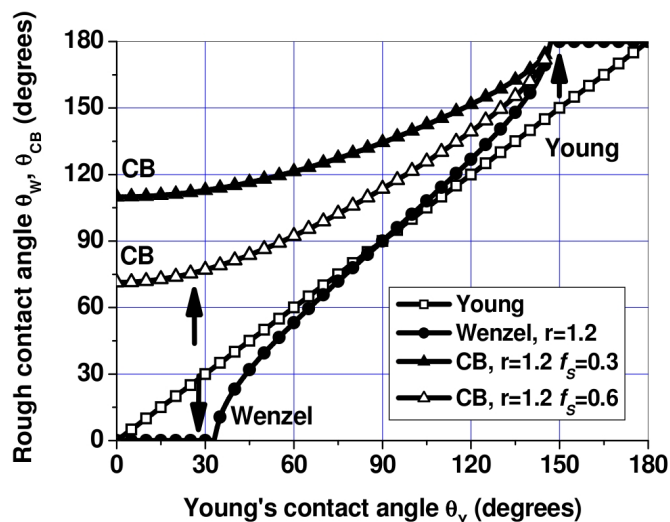


Figure 6: Differences of contact angle between Wenzel's and Cassie-Baxter's model for different values of Young's flat surface contact angle [7].

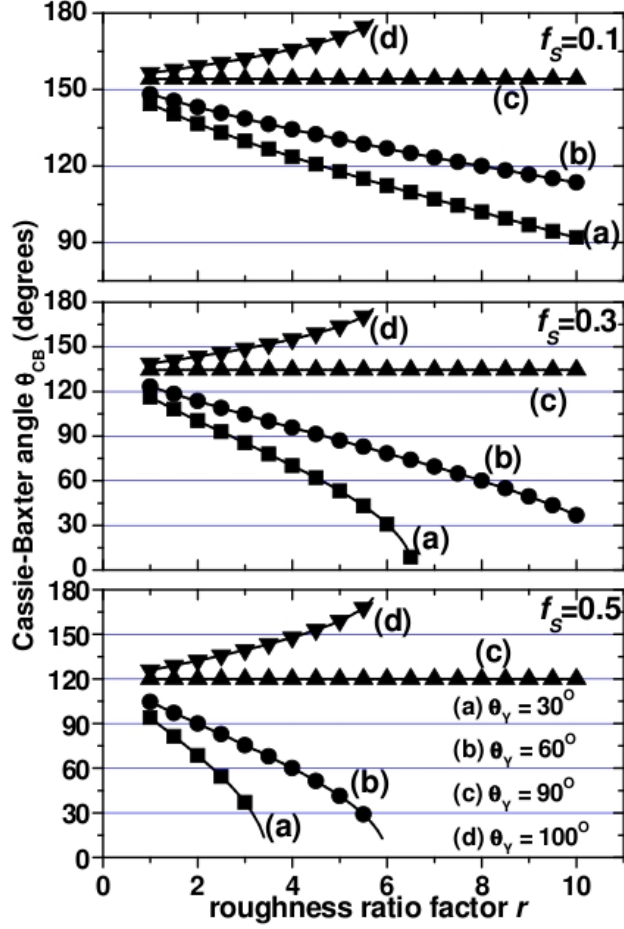


Figure 7: Cassie-Baxter angle as a function of roughness  $r$ , for various values of Young's flat surface angle  $\theta_Y$  and  $f_s$ . Note that it is not possible to turn hydrophobic surfaces ( $\theta_Y > 90^\circ$ ) into hydrophilic surfaces ( $\theta_{CB} < 90^\circ$ ) [5].

### 2.3 Bouncing droplet

When a liquid drop is falling on a hydrophobic surface, there are multiple scenarios possible for what happens after initial contact. Depending on parameters such as surface properties, fluid properties, droplet size and impact speed, the droplet will bounce, stick to the surface or splash. The latter is the fragmentation of a part of the droplet into multiple smaller droplets. The exact mechanism of energy transfer and dynamical behavior of the droplet impact are quite complex and probably still not fully understood [19].

Rebounds of droplets are only possible if impact speeds are high enough. We assume a simple model of energy transfer between kinetic and potential energy. When a droplet impinges a surface, its inertia forces the droplet to spread out over the surface. The

kinetic energy of the droplet is converted into surface energy, which is used for retraction and rebound of the droplet. Since we are dealing with hydrophobic surfaces with low surface energies, we assume that the dissipation of energy due to friction can be neglected. Because of contact angle hysteresis, in the process of expansion and retraction the droplet can store some energy. The kinetic energy of a drop has to exceed this energy to be able to bounce. The stored surface energy is estimated by Eq. 10 in which  $R$  is the radius of the droplet [15].

$$E_{stored} = \lambda R^2 |\cos\theta_A - \cos\theta_R| \quad (10)$$

The kinetic energy of the droplet is stated as

$$E_{kinetic} = \rho R^3 V^2 \quad (11)$$

in which  $\rho$  is the fluids mass density. The critical impact velocity for a droplet to bounce is therefore given by Eq. 12 [15].

$$V = \left[ \frac{\lambda |\cos\theta_A - \cos\theta_R|}{\rho R} \right]^{1/2} \quad (12)$$

Usually in literature, the droplet impact dynamics are characterized using dimensionless quantities. In this report drop dynamics will be discussed in terms of Weber number  $We$  and Reynolds number  $Re$ . The Weber number gives the ratio between kinetic energy and surface energy as shown in Eq. 13) and the Reynolds number gives the ratio of the inertial force and the viscous force, shown in Eq. 14 in which  $\eta$  is the fluid viscosity.

$$We = \frac{\rho R V^2}{\lambda} \quad (13)$$

$$Re = \frac{\rho R V}{\eta} \quad (14)$$

With increasing Weber number, the behavior of an impinging droplet changes. Tsai et al. found that in the range of small Weber numbers, the droplet behavior after impact is independent of detailed changes in surface roughness [24]. Using superhydrophobic surfaces and water drops, they found for  $We \leq 2.5$  that increasing impact speeds lead to a gradually change in impact behavior. Starting at the lowest Weber number they successively found the droplet to behave as a Fakir droplet (in Cassie-Baxter state), to completely rebound, to be pinned to the surface displaying vibrations (Wenzel state) and to partially rebound, see also Figure 8. When the droplet is gently deposited, such as in the lowest Weber numbers, the droplet maintains a Cassie-Baxter state, with air trapped underneath the drop. Therefore during the whole impact process, the droplet displays a high contact angle. This distinguishes it from the Wenzel state, at higher impact speeds. In the latter case, the liquid penetrates the surface structures and becomes more sticky. The measured contact angles during impact will be smaller. In the case of partial rebound, a small part of the droplet transits into Wenzel state and sticks to the surface, whilst the rest of the droplet splits off and rebounds of the surface. It has been observed that at second rebound, the large split off drop reunites with the smaller droplet

and pulls it out of Wenzel state [8]. Usually the transition between different phenomena is smooth, with overlaying regions of Weber numbers. This illustrates the complexity of the impact process and indicates that there are other factors which influence the droplet behavior.

Beyond a certain Weber number, the deformation is sufficiently large that after impact a cavity is formed at the center of the drop and the liquid takes a toroidal shape in the spreading stage. For  $2 \leq We \leq 10$  Tsai et al. observed a small air bubble trapped inside the cavity during retraction, since the top of cavity retracted faster than the bottom [24]. For lower impact speeds,  $We = 5.3$ , this deformed and elongated the droplet at lift off. At higher impact speeds,  $We = 7.7$ , the fast collapse of the cavity caused the ejection of a small high speed water jet. Also at higher Weber numbers the surface structure start to play a more important role in impact behavior. For Weber numbers above 10 (in the higher range), phenomena that occur are a sticky droplet in Wenzel state, the formation of a few satellite drops while the main impact reveals a partial rebound and a wetting ( $\theta < 90^\circ$ ) droplet in Wenzel state. These phenomena are displayed in order of advancing impact speed, see also Figure 8.

When Weber numbers increased above 120, splashing occurred. This is the effect that the droplet breaks into multiple satellite drops during the spreading and retraction phase. The cause for this to happen is probably a combination of compressed air at the leading edges of the spreading droplet which forces the spreading front upwards and the surface tension of the fluid which tries to keep to droplet intact. When the stresses due to these two attributions become comparable, the droplet is expected to become unstable and break up into smaller droplets. Experiments performed in vacuum chambers showed that no splashing occurs at lowered pressure for dry smooth surfaces [28]. On micro- and nanostructured surfaces however, the lowered pressure shows no effect on splashing [24].

The influence of viscosity on droplet impact is a subject on which hardly any publications have been made. Most of the research that has been performed on the subject of bouncing droplets use water for a liquid. However there has been some research on the influence of surface temperature on droplet impact dynamics. Recently Alizadeh et al. showed that for hydrophilic surfaces with a decreased temperature of  $-15^\circ\text{C}$ , the spreading and retraction of an impinging droplet with a temperature of  $22^\circ\text{C}$  was slowed down considerably [4]. The explanation for this is, that even during the short period of contact time, a small layer at the lower side of droplet is cooled down, since it is in direct contact with the surface. Most of the energetic losses due to shear stresses at the surface occur in this region close to the surface. With lower temperatures, the fluid viscosity increases, resulting in higher losses, thus less available energy for the retraction and rebound of the droplet. On superhydrophobic surfaces, no influence from surface temperature was observed. The explanation for this is the thin film of air, which is formed between the surface and the impacting droplet and limits the cooling of the droplet [4]. Bearing this in mind, Eq 12 should be applied carefully on fluids with a higher viscosity.

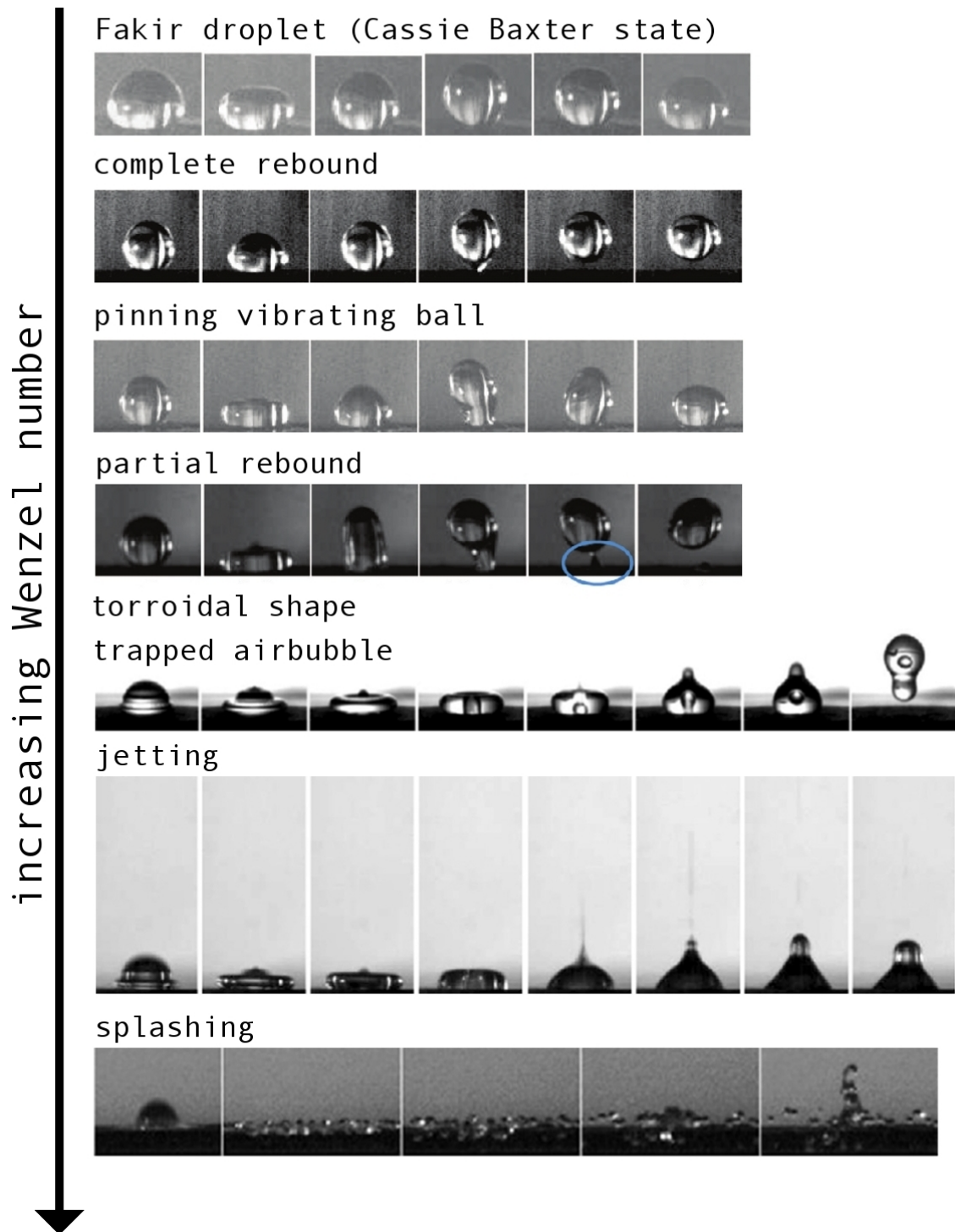


Figure 8: Different phenomena of droplet impact as seen by Tsai et al.. Foto's adapted from [8, 24].

### 3 Experimental

Multiple series of polydimethylsiloxane (PDMS) samples with differing micro-level surface structures have been analyzed and tested on hydrophobic and omniphobic properties. The surfaces were immersed in hydrophobized aluminum nano-particles to enhance the hydrophobic properties of the samples.

#### 3.1 Sample preparation

The process of sample creation holds three major steps. At first the mold is treated. On the mold there are different patterns of dimples. When PDMS is cast using the mold, this results in carpet-like PDMS samples. Finally these samples receive a special coating to enhance hydrophobic capacities.

##### Mold

The PDMS samples were created using a mold provided by the company Lightmotif, a spin-off from the University of Twente. The mold is made out of stainless steel and holds 12 samples with different micro-level surface structures. The samples on the mold consist out of straight dimples with a depth between 60 and 100  $\mu m$ . The dimples are created using laser pulses and are positioned in a hexagonal pattern. The depth of the dimples vary with the number of laser pulses per dimple. More pulses means a deeper dimple. The surface parameters for each sample are displayed in Table 1. The PDMS samples will have the mirrored image of the mold, so the dimples will become pillars. The distance between pillars is constant, but differs per sample. The stainless steel mold was treated using an O<sub>2</sub> plasma cleaner. This cleans the surface and removes contaminants, ensuring a nice smooth surface for the PDMS to be molded on [2].

Table 1: Design parameters for each sample. Spacing is the distance between the center of the dimples in the hexagonal pattern.

Sample	Spacing [ $\mu m$ ]	Pulses
1	22	6000
2	28	6000
3	33.5	6000
4	39	6000
5	22	4500
6	28	4500
7	33.5	4500
8	39	4500
9	22	3000
10	28	3000
11	33.5	3000
12	39	3000

## PDMS

PDMS is used as a substrate in this research for its excellent properties as a micro-molding material. It is also non-toxic and its surface chemistry can be controlled by reasonably well-developed techniques. This is especially valuable in later stages of this study. Thereby because it is elastomeric, it can conform to non-planar surfaces and it releases from delicate features of a mold without damaging them, or itself [18].

The PDMS used in this research is widely used and industrially produced. It consists of two different liquid substances, a base polymer and a curing agent. The two ingredients are mixed and stirred in a weight ratio of 10:1. Typically between 40 and 50 *gram* of base resulted in sample thickness of somewhat about 4 *mm*. This proved to be an ideal thickness for contact angle measurements. After stirring, the PDMS mixture was put in a vacuum chamber until the gross majority of the air bubbles in the liquid where vanished and the PDMS had turned into a clear liquid. After this the clear liquid PDMS was poured over the steel mold placed in a petri dish. Again this was put in a vacuum chamber to suck out the remaining air. Usually vacuum times where around 15 minutes. Then this was put in the oven at 100°C for one hour. During this time the liquid PDMS cured, forming a rubber like, transparent solid. After cooling down the PDMS was carefully subtracted in one direction of the mold. The dimples on the mold are pillars on the PDMS. Due to their height, the pillars will not maintain an upright position, but tumble over, see Figure 9. At higher densities the pillars are to close together and tend to stick to each other. This results in ‘Christmas tree’ like shapes, as can also be seen in Figure 9 Sample 5. This might turn out to be a disadvantage, since the resulting defects in the structure are relatively large compared to the spacing between pillars.

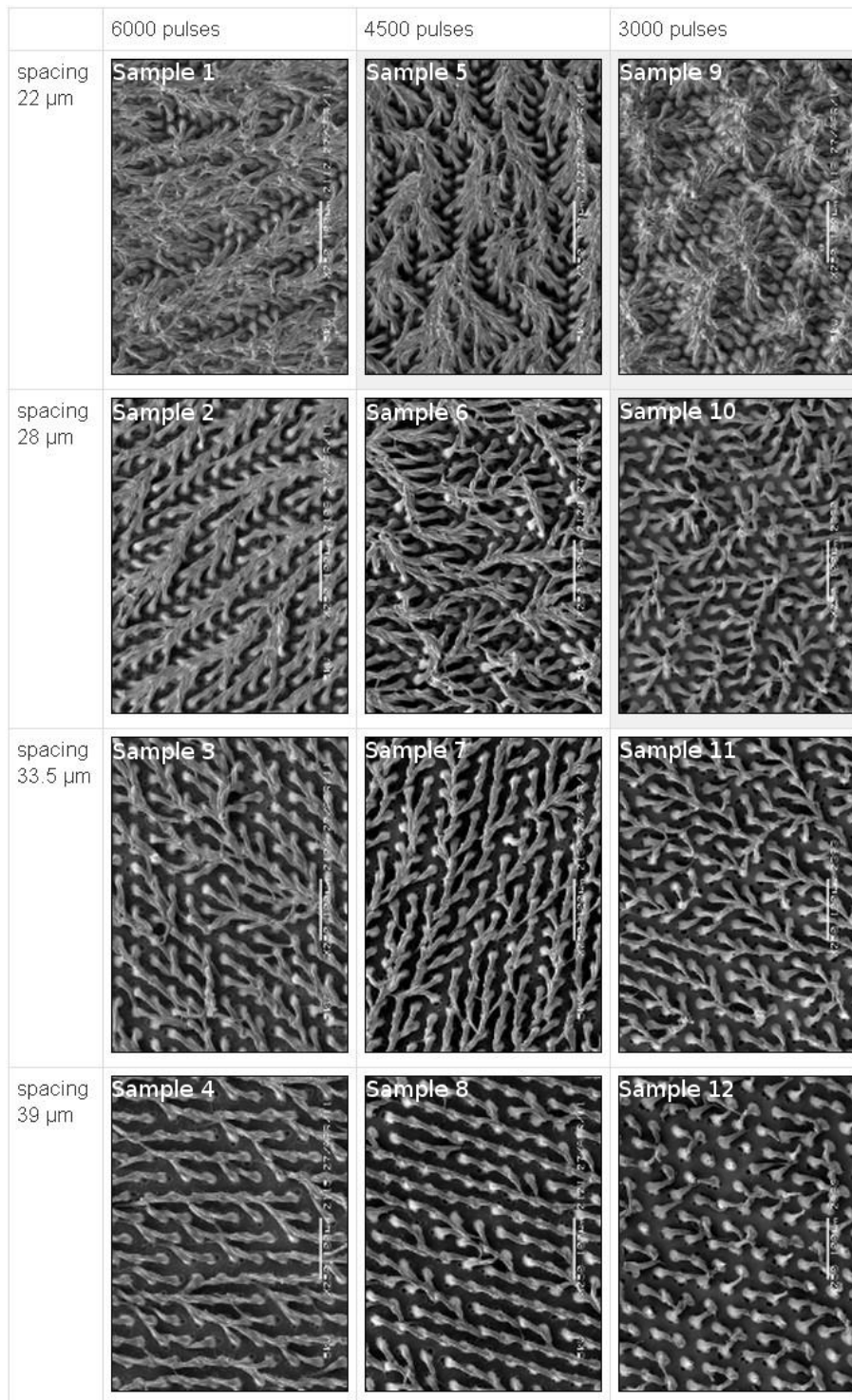


Figure 9: An overview of the PDMS samples, sorted by spacing and pillar length. Note the irregularities and large gaps for the samples with low spacing.

## Aluminum particles

On the PDMS we applied a hydrophobic coating. This consisted out of aluminum nano particles with a typical diameter of  $800\text{ nm}$ , thus it can be seen as aluminum powder. This powder was made hydrophobic using fluorosilane, FOTS. A coating of FOTS provides very hydrophobic and oleophobic surfaces [30]. The aluminum powder was emulsified in hexane, together with a few drops of FOTS. This was put in an oven at  $120^\circ\text{C}$  for about two hours, until all the hexane was evaporated. The resulting hydrophobic powder was emulsified in chloroform. Chloroform is a high-solubility solvent that causes the PDMS to swell and can be used to extract un-cross-linked PDMS from the bulk polymer [13]. This process softens the PDMS at the surface, causing the aluminum particles to stick to the surface. When the chloroform evaporates, the PDMS will shrink to its original size again. The majority of aluminum particles will stick very tightly to the surface, whilst excess particles can easily be removed using sticky tape.

## 3.2 Experimental setup

### Hysteresis

Contact angle measurements for hysteresis were carried out at room temperature on a Dataphysics, OCA 15 plus instrument (Dataphysics Instruments GmbH, Germany). Water and ethyleneglycol were used as liquids. Water has a surface tension value of  $72.13\text{ mN/m}$  ( $25^\circ\text{C}$ ) and is used to estimate the degree of hydrophobicity of the surface. Ethylene glycol has a surface tension value of  $47.3\text{ mN/m}$  ( $25^\circ\text{C}$ ) [3]. This is significantly lower than the value for water and gives a better indication of the oleophobicity of the surface. For the hysteresis measurements there was placed a  $3\text{-}5\text{ mL}$  droplet on a surface. With the needle used for deposition still sticking in the droplet,  $7\text{-}10\text{ mL}$  of fluid was added and removed. The measurements were repeated on different areas on the sample and average values were calculated. This to give a better insight in the overall hydrophobicity of the sample. Thereby it is not unusual that comparable hysteresis measurements differ a few degree in results. The contact angles were measured at a constant time interval during the process of hysteresis using the Dataphysics software. This software determines the shape of the drop using the differences in light intensity between the droplet and its surroundings. It fits a circumferential line on the droplet and uses this to determine contact angles. Practice showed that the PDMS samples were to have a minimum thickness of about  $4\text{ mm}$  for the software to distinguish the droplet from the surface beneath it.



Figure 10: Image from the Dataphysics OCA. Shown is a water droplet of about  $4\mu\text{l}$  with the syringe used for deposition still sticking in it.

### Falling droplet

The setup for the falling droplet uses also the Dataphysics OCA 15 plus. From a certain height, droplets were dropped on top of the surface. The motion of the drops were filmed using a high speed camera <sup>1</sup> with a framerate of 500 fps. In this experiment, both water and ethylene glycol were used as liquids. Droplet volumes varied between 6 and 14  $mL$ , depending on the volume needed to detach from the syringe.

### 3.3 Data processing

The data is processed using Matlab, ImageJ, OriginPro 8 and SciDAVis. ImageJ is software used for video and photo analysis. Origin and SciDAVis are both software packages for graphical representation and processing of scientific data. Matlab is a program used for numerical computing and widely used by scientists, engineers and students.

### Hysteresis

From the data output of the Dataphysics software, the contact angles were imported in Origin and smoothed using a Savitzky-Golay smoothing filter [22]. Matlab was used to determine the average values and standard deviations. The resulting error bar plots were made using SciDAVis as shown in Figure 12.

### Falling droplet

The video output from the high speed camera was analyzed with ImageJ. The thickness of the needle and the spacing between two neighboring samples were taken as references in the image to determine the distance between the needle tip and the surface.

---

<sup>1</sup>Mikrotron GmbH MotionBLITZ EoSens mini2

## 4 Results and Discussion

The hysteresis measurements and the analysis of falling droplets are performed as described in the experimental section above. Water and ethylene glycol were used as liquids in the experiments. The results discussed here from hysteresis measurements were all obtained using ethylene glycol. For the bouncing drop experiments both liquids were used.

### 4.1 Hysteresis

The first series of experiments were performed to discover a connection between pillar density and surface hydrophobicity. Typical hysteresis curves found looked like the one in Figure 11. The upper left of the curve is a plateau phase corresponding to the advancing contact angle  $\theta_A$ , on the lower right is another plateau phase corresponding to the receding contact angle  $\theta_R$ . The difference between these two angles is the amount of hysteresis.

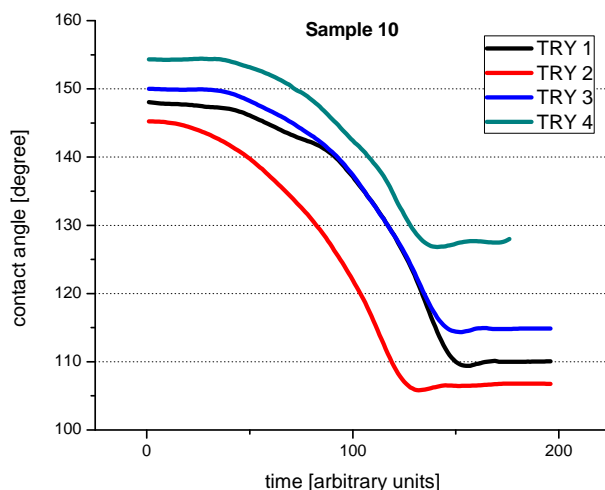


Figure 11: Typical hysteresis curve for ethylene glycol on micropatterned PDMS. The graph is cropped such that the left side shows the plateau for the advancing contact angle and the right side shows the plateau corresponding to the receding contact angle.

On every sample there were performed 4 - 6 measurements. On samples 1-4 the PDMS turned out to be too thin for reliable experiments. Due to poor contrast between droplet and surface, the Dataphysics OCA used for contact angle measurements had trouble fitting a line around the droplet. The various measurements were conducted on different parts of the sample and are denoted try in the graphs. The hysteresis curves

were plotted just like Figure 11. Out of convenience these are left away, the hysteresis results are represented with an error bar plot in Figure 12. The measured contact angles were ranging between  $100^\circ$  and  $150^\circ$ . To compare these results with water, 5 contact angle hysteresis measurements were performed on samples 10 and 12. The contact angle hysteresis for sample 10 was measured to be  $7.2^\circ \pm 5.7^\circ$ . For sample 12 this turned out to be  $2.6^\circ \pm 2.3^\circ$ . All the measurements were in the contact angle range between  $140^\circ$  and  $160^\circ$ , thus on the edge of superhydrophobicity.

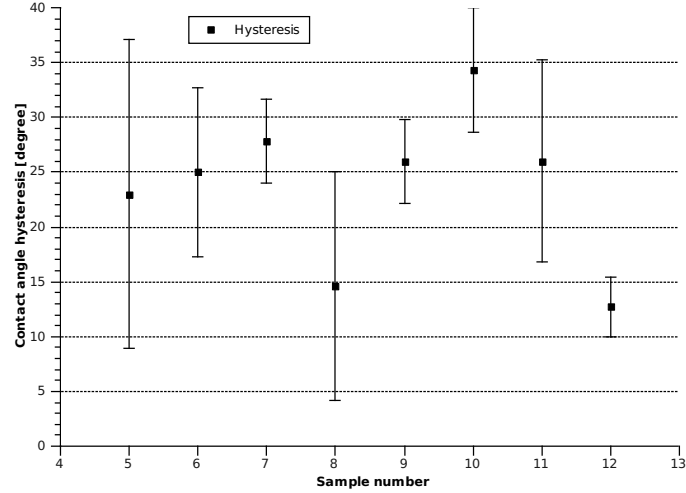


Figure 12: Error bar plot of sample 5 - 12 for the first series of tests. Average values and standard deviations from 4 - 6 contact angle hysteresis measurements for ethylene glycol on micropatterned PDMS.

After this first series of experiments it was concluded that samples 8 and 12 showed best results. The other samples displayed significantly larger hysteresis contact angles. Sample 4 and 8 both have the lowest pillar density. Probably the higher pillar densities result in pillars sticking together and forming to large discontinuities in the surface. This can be seen in Figure 9 and corresponds with the results from hysteresis measurements plotted in Figure 13. These larger discontinuities make the droplet (locally) transit from Cassie-Baxter to Wenzel state, resulting in larger adhesive forces between the liquid and solid. From Table 1 it can be seen that sample 4 has the same pillar density as 8 and 12. After this it was decided to focus on samples 4, 8 and 12.

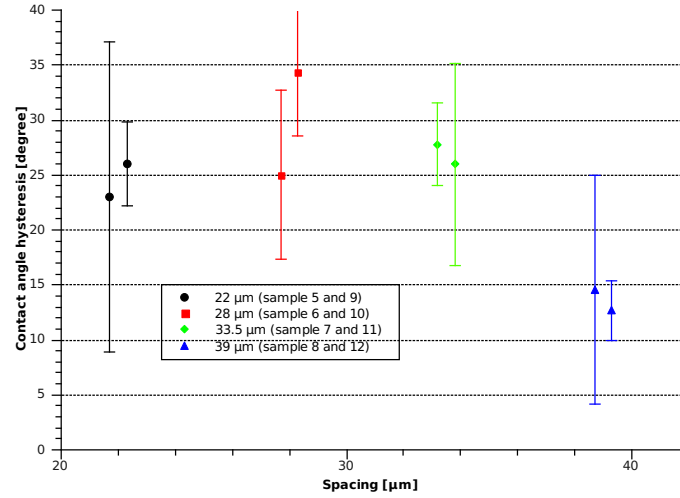


Figure 13: Average contact angle hysteresis values with standard deviations plotted versus the sample pillar spacing of ethylene glycol on PDMS.

For the second series of experiments new PDMS samples were created. The hysteresis measurements were at first performed on clean samples. After this the same samples were treated with Aluminum particles forming a hydrophobic coating. Then again experiments were performed, showing enhanced results for samples 4 and 8, see Figure 14. What stands out is that if the hysteresis curves from the same sample numbers are compared, one of them is coated, the other one is clean, is that the curve for the coated sample looks less smooth than the curve for the clean sample. This was to be expected, since the added particles increase the roughness of the surface. The discontinuities on the surface causes pinning of the contact line. This means that the liquid-vapor-solid interfaces, which moves during hysteresis, gets stuck behind regularities during movement. Instead of a smooth movement over a flat surface, the contact line ‘jumps’ from irregularity to irregularity [9]. The increased roughness due to the added particles enhances this effect.

What stands out is are the differences in contact angle hysteresis for the first and the second series of samples. The results for the second series of measurements are much improved compared to the first series. This is illustrated in Figure 14. Possibly this is because the production of the second series of PDMS samples was more successful after gaining some experience producing the first samples. Therefore samples from the first PDMS serie where to have more defects in the surface structure than the second series. This becomes clearer after observation of the SEM images from the first series of PDMS samples. As can be seen in Figures 17 and 18 in Section A, there are a lot of defects on the surface in the form of pillars sticking together and even missing pillars. The latter is very clear in Figure 18, showing a whole area of missing pillars. Explanations for this possibly are that the dimples on the mold did not fill properly, or that the pillars stayed behind in the dimples when the PDMS was subtracted from the mold. In the case of

the latter however, this would mean that the second series of samples would show about equally results as in the first series. Observation of Figure 14 shows however that at least one of the samples shows significant differences between series one and two.

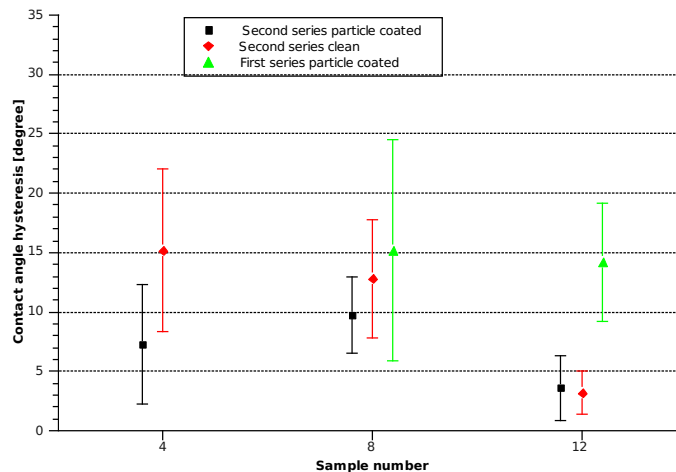


Figure 14: Error bar plot for samples 4, 8 and 12 out of both series. Measurements performed on micropatterned PDMS using ethylene glycol. Note the large differences between series 1 and 2 and the improvement due to coating

## 4.2 Bouncing Droplet

Before we started with the first falling droplet experiments on the first series of samples, the results from the hysteresis measurements were not processed yet. By sliding droplets over the surfaces we were able to observe pinning of the droplet and its transition into Wenzel state. Using this method we found on sample 6 an area that showed good hysteresis results. We decided to use this area for our bouncing droplet experiments to get a first impression of the performance of our surfaces.

We started with water and tried to see how high we could go before the droplets would not bounce anymore. Soon it turned out that with our setup we could not reach heights sufficiently such that the impacting droplet would stick to the surface and at the same time still give a good image of the droplets behavior. Ethylene glycol has a lower surface tension than water and provided us with higher Weber number for the same impacting speed, also see Eq. 13. At the same time, ethylene glycol also has a higher viscosity than water. The value for ethylene glycol is  $16.06 \text{ mPa} \cdot \text{s}$  ( $25^\circ$ ) and for water this is  $0.890 \text{ mPa} \cdot \text{s}$  ( $25^\circ$ ) [12].

The falling droplet results for water on sample 6 are displayed in Figure 21 in Section A. The droplet falling height varied between  $7.5$  and  $40.9 \text{ mm}$ , with corresponding impact speeds (calculated using elementary physics) ranging between  $0.38$  and  $0.90 \text{ m/s}$ . The droplet diameters were measured to be about  $1.76 \pm 0.02 \text{ mm}$ . We did not observe

complete sticking of the droplet during these experiments. For the lowest impact speeds of  $0.38 \text{ m/s}$  a restitution coefficient of 0.5 was observed. With increasing impact speeds this lowered to about 0.2 for the highest impact speed. All the rebounding droplets displayed vibrations, probably indicating some partial pinning to the surface. Non of the droplets observed stucked fully to the surface.

The falling droplet results for ethylene glycol on sample 6 are displayed in Figure 15. The range of falling height for these droplets is from  $3.1$  to  $17.0 \text{ mm}$  with corresponding impact speeds ranging between  $0.24$  and  $0.58 \text{ m/s}$ . The droplet size was measured to be  $2.1 \pm 0.1 \text{ mm}$ . The behavior of the ethylene glycol was less turbulent than the water. It showed only little vibrations and no phenomena such as high speed jetting, trapped air bubbles or satellite droplets being emitted from the main drop. Comparing Figure 21 with 15 shows that ethylene glycol features much lower Reynolds numbers for the same Weber numbers. Since the loss of energy due to viscous effects is much higher for ethylene glycol than it is for water, as explained in Section 2.3, the higher viscosity of ethylene glycol probably explains the difference in behavior.

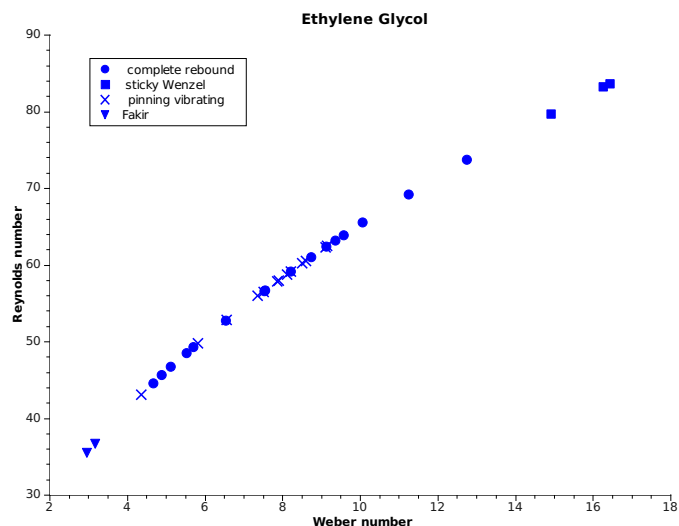


Figure 15: Droplet impact behavior for samples 6 of the first series using ethylene glycol. Falling heights range from  $3.06$  till  $16.95 \text{ mm}$ , impact speeds range from  $0.24$  till  $0.58 \text{ m/s}$  with a droplet diameter of  $2.1 \pm 0.1 \text{ mm}$ . Highest (partial) rebound was observed at  $11.6 \text{ mm}$  with an impact speed of  $0.48 \text{ m/s}$ .

Since samples 4, 8 and 12 from the second series of samples showed to have nice oleophobic surface properties, it was to be expected that these would also perform well on the falling droplet experiments. The bouncing experiments for the second series of samples were therefore performed on these three samples only. To get an overall view of the surface properties, the droplet impact was studied on different locations of the sample. Already during experiments it became clear that not everywhere on the sample the behavior of the impinging droplet was equal. The way we performed the experiments

was that we started at a relatively low height. When the droplet was seen to rebound, the falling height was increased, or the location of the drop impact was moved. In the case of a non rebounding droplet, the sample was moved a little to change the impact location. If then rebound would occur, the experiments would be continued in the same manner as before. Otherwise the bouncing height would be lowered a bit. It happened frequently that a change of location changed the droplets behavior.

Figure 16 shows a graph of the droplet impact behavior for samples 4, 8 and 12. It looks a little chaotic, since it covers a the data of 3 different samples. The plots for the individual samples are presented in the Appendix, Section A. An overall observation however that for the highest Weber (and Reynolds) numbers, sample 12 still (partly) rebounds. In the transition region between pinning vibrating and complete rebounds (Weber numbers around 15) for sample 12, the the other samples show a complete Wenzel state.

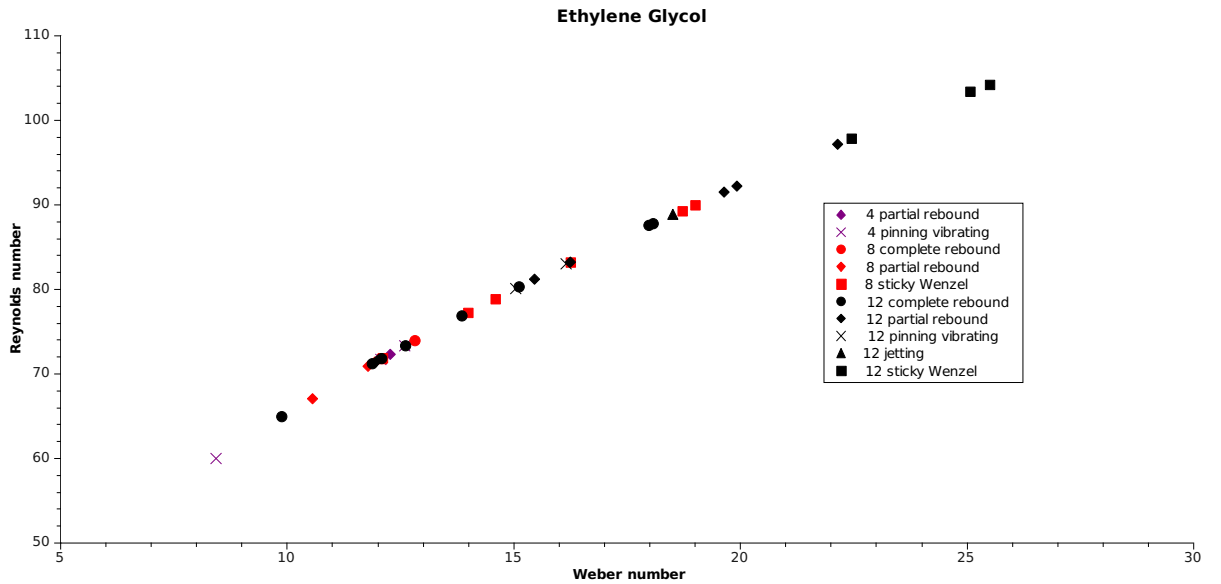


Figure 16: Droplet impact behavior for samples 4, 8 and 12 using ethylene glycol. Falling heights range from 8.7 till 25.8  $mm$ , impact speeds range from 0.41 till 0.71  $m/s$  with a droplet diameter of 2.1  $\mu m$  0.1  $mm$ . Highest (partial) rebound was observed at 12.3  $mm$  with an impact speed of 0.49  $m/s$ .

The expected droplet impact behavior for water is as in Figure 8 and as described in section 2.3. However as stated above, the droplet behavior of ethylene glycol is different than that of water. Therefore what is to be expected for the lowest Weber numbers is a Fakir droplet in Cassie Baxter state, while this is merely just a gentle deposition of the droplet on the surface. A little increase in Weber number would probably show a complete rebound of the droplet. During the complete impact of spreading and retraction of the droplet, it will maintain its Cassie Baxter state. Since the impact speeds is high enough, it contains enough kinetic energy to overcome the energy boundary required for rebounding, see also Eq. 12. An increase of impact speed will probably result in a partial transition into Wenzel state for the droplet. The pressure due to impact of the drop is locally (at the center of the drop) high enough to force it into Wenzel state. The kinetic energy of the rebound won't be high enough to pull this part of the droplet out of it's Wenzel state or to simply tear the droplet apart. Therefore it will be prevented from rebounding. For higher impacting speeds the droplet does contain enough kinetic energy to to pull itself out of Wenzel state or to overcome the boundary needed to break the adhesive forces inside the droplet. This is shown nicely in Figures 19 and 20, see Section A. These show comparable droplet impact for samples 8 and 12. On sample 12 a complete rebound is observed, whilst on sample 8 a small amount of fluid sticks to the surface. Probably with further increasing impact speeds, a larger part of the droplet transits into Wenzel state, until the droplet won't rebound anymore, but maintains a sticky Wenzel state. The transitions between these phenomena will probably be smooth, with some overlay. Mainly because the surfaces are not uniform, but also because of the complexity of the process of droplet impact, which makes it difficult to exactly reproduce results.

Table 2: Critical Weber number,  $We_c$ , for which a complete rebound transits to a sticky Wenzel droplet. The critical number is taken to be the average between the highest Weber number for complete rebound and the lowest Weber number for which sticky Wenzel occurs.

Sample	Serie	Liquid	$We_c$
6	1	water	>9
6	1	ethylene glycol	13.9
4	2	ethylene glycol	12.5
8	2	ethylene glycol	13.4
12	2	ethylene glycol	20.3

Figures 22, 23 and 24 in Section A display the droplet impact phenomena for samples 4, 8 and 12. With sample 4 we soon realized that it would not give us best results, since it mainly displayed pinning and that it was very difficult to obtain a rebound.

Sample 8 gave some more interesting results. Still the region for complete rebound is not very wide. This is an important region though, since after the rebound, the restitution coefficient is quite low for ethylene glycol. This means that there is no

second rebound, of even pinning vibrating. After the first rebound the impact usually looks like a Fakir droplet.

For sample 12, between Weber numbers 15 and 20, there is a transition region. It displays complete and partial rebounds as well as pinning vibrating drops. Since both the higher and the lower Weber region display more or less unambiguous behavior, it can be seen as that this transition region gives an indication of the uniformity of the surface. On a uniform hydrophobic surface, the transition region between impact phenomena should be small. For non uniform surfaces, on which the hydrophobicity differs a bit per location on the surface, the transition region measured over the entire surface will be wider.

For each sample the transition region was determined to define a critical Weber number  $We_c$ . To obtain this critical number, the average value between the highest Weber number for complete rebound and the lowest Weber number for which sticky Wenzel occurs, is taken to be the critical Weber number<sup>2</sup>. The resulting critical Weber numbers are displayed in Table 2.

---

<sup>2</sup>For sample 4 no complete rebound or sticky Wenzel occurred, therefore  $We_c$  is taken to be the average value between partial rebound and the value of the next pinning vibrating

## 5 Conclusions and Recommendations

In this research an analysis has been made of the hydrophobic and oleophobic properties of a number of patterned PDMS samples. The samples are comparable in design, since they are all build up out of straight pillars. These pillars fall over and form a ‘fur’ like structure. The samples differ in pillar height and spacing between the pillars. For the highest density of pillars, with spacing 22 en 28  $\mu m$ , the pillars tend to stick together, resulting in large gaps in the structure, as can be seen in Figure 9. This resulted in pinning and relatively high values of hysteresis. The remaining focus of this research was therefore on the configurations with lower pillar densities. For further research, it should be interesting to consider samples with an even lower pillar density, since the combination of lowest pillar density and smallest pillars provided us with best results, with contact angle hysteresis angles lower than  $5^\circ$  using ethylene glycol. Also for ethylene glycol, the measured contact angles were ranging between  $100^\circ$  and  $150^\circ$ , which are good results in terms of oleophobicity.

The uniformity of the surfaces provided some problems and should be a very interesting topic for future research. During experiments it was already noticed that different areas of the samples showed different behavior in terms of contact angle hysteresis and rebound heights. This is displayed in Figure 12, which features some very large deviations in contact angle hysteresis. SEM<sup>3</sup> images showed that there were indeed large variations in surface geometry.

On the surfaces a coating of aluminum particles was applied to enhance its hydrophobic properties. These particles were applied on the PDMS surface using chloroform. This is effective, but the dosage and spreading are hard to control. SEM images showed accumulations of particles on some parts on the surface, whilst on other parts almost no particles were present. This can perhaps be improved by using electrospraying, a technique related to electrospinning. However, referring to Figure 14, it is safe to state that the aluminum particle coating did positively influence the hydrophobic and oleophobic properties of the samples.

The experiments with the bouncing droplets turned out to be very interesting. Droplets of ethylene glycol were seen to rebound after falling from heights up to 12.3  $mm$ . Due to restrictions in our setup, we were not able to reach such a limit for water, but it is expected to easily exceed the 40  $mm$  we could measure. The majority of the experiments were conducted using ethylene glycol as a liquid, which is quite unusual in the field of bouncing droplets. This provides a research window for the influence of viscosity on surface properties and impinging droplets.

The most important conclusion that can be drawn from this research, is that oleophobic surfaces can be produced using simple techniques such as molding. This brings us a step closer towards the production of repellent surfaces which can form the basis of a new wide variety of products and applications.

---

<sup>3</sup>Scanning Electron Microscope

## A Remaining Pictures and Graphs

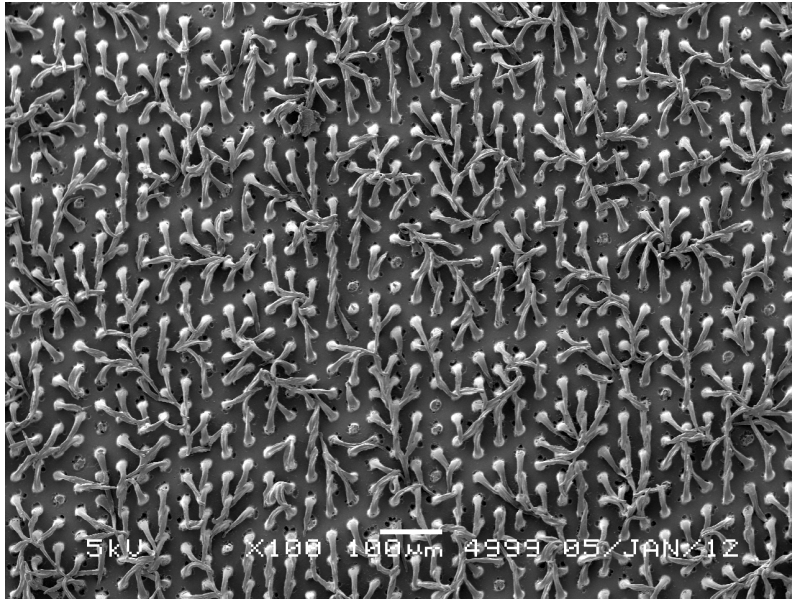


Figure 17: SEM image from first series of samples. It shows the non-uniformity of the surface, with pillars sticking together and even some missing pillars.

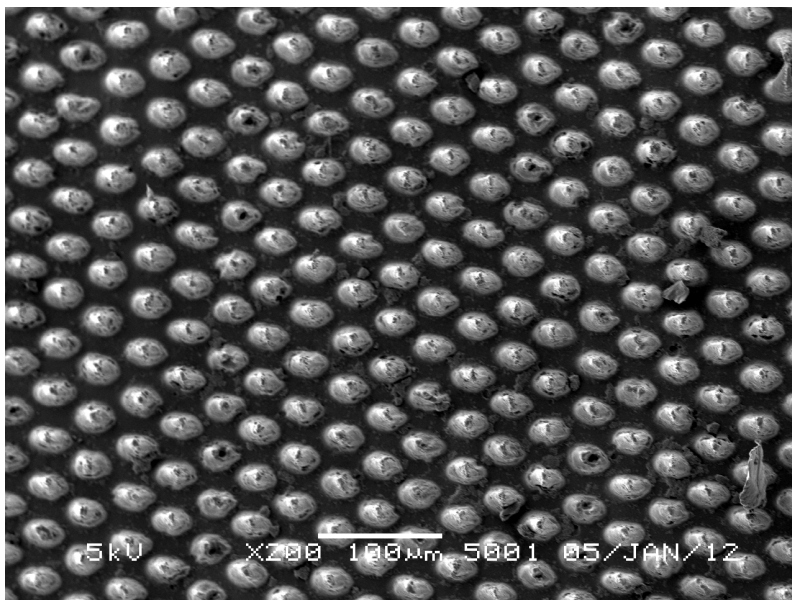


Figure 18: SEM image from first series of samples. It shows a region where almost all pillars are missing, probably due to bad filling of the dimples on the mold.

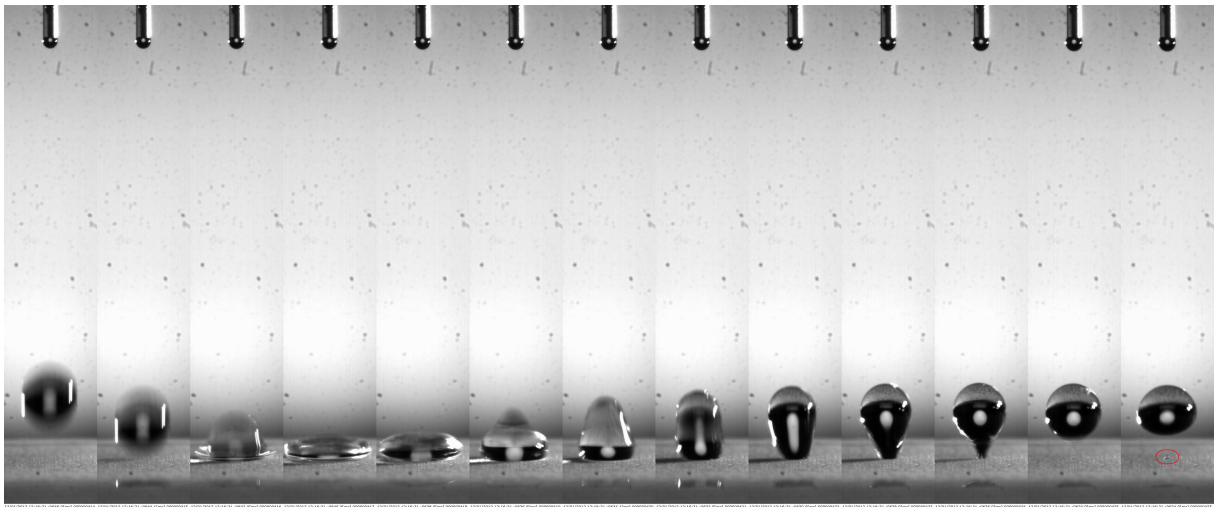


Figure 19: A drop of ethylene glycol falling on sample 8. A small amount of liquid remains behind due to locally transition into Wenzel state, whilst the rest of the fluid rebounds from the surface.

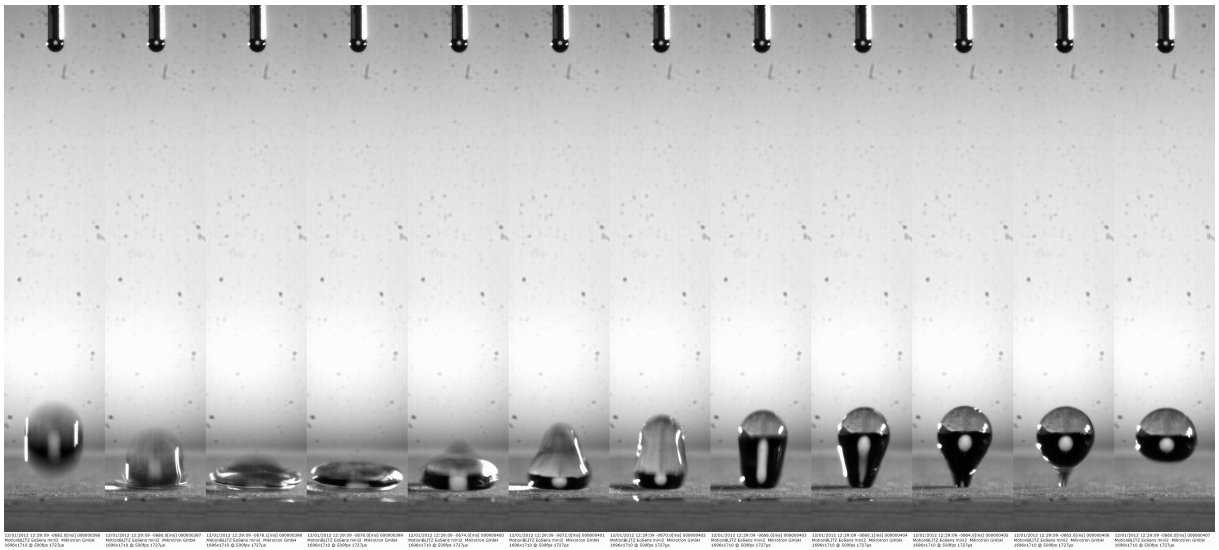


Figure 20: A drop of ethylene glycol falling on sample 12. This is a complete (clean) rebound.

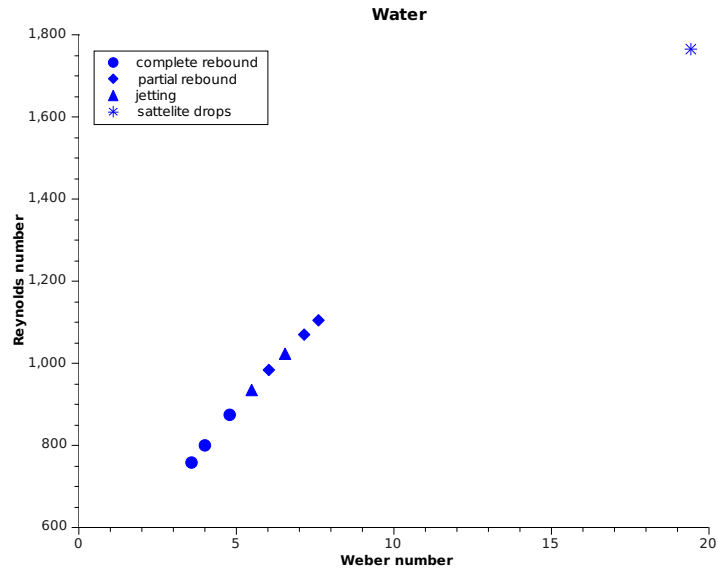


Figure 21: Droplet impact behavior for samples 6 of the first series using water. Falling heights range from 7.5 till 40.62 mm, impact speeds range from 0.38 till 0.89 m/s with a droplet diameter of 1.8 mm. Highest (partial) rebound was observed at 40.62 mm with an impact speed of 0.89 m/s.

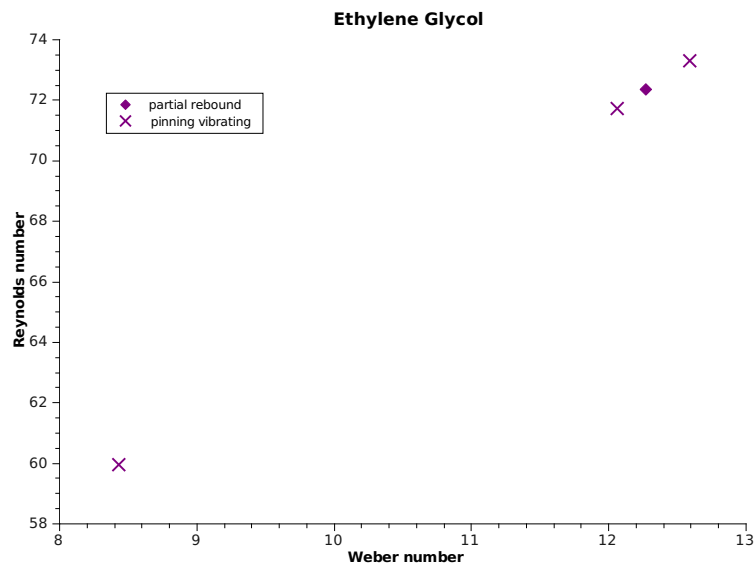


Figure 22: Sample 4. Falling heights ranging from 8.7 till 13.0 mm, impact speeds range from 0.41 till 0.50 m/s with a droplet diameter of  $2.1 \pm 0.1$  mm. Highest (partial) rebound was observed at 12.7 mm with an impact speed of 0.50 m/s.

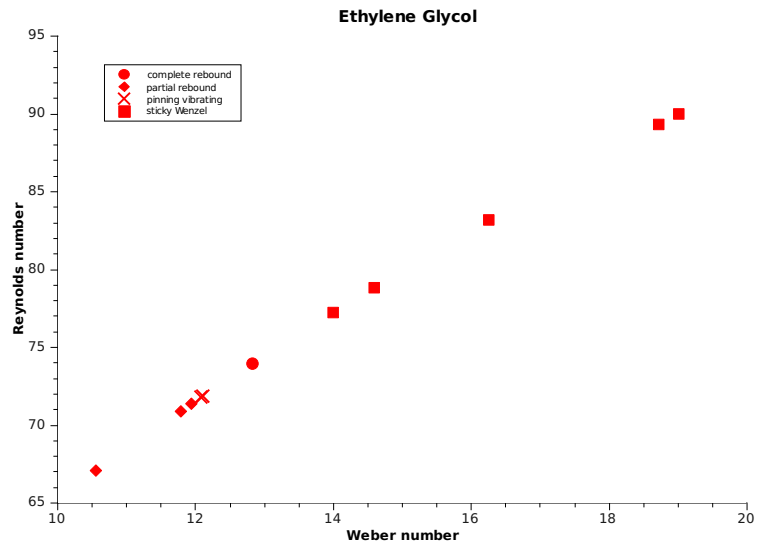


Figure 23: Sample 8. Falling heights ranging from 10.9 till 19.6 mm, impact speeds range from 0.46 till 0.62 m/s with a droplet diameter of  $2.1 \pm 0.1$  mm. Highest (partial) rebound was observed at 20.6 mm with an impact speed of 0.64 m/s.

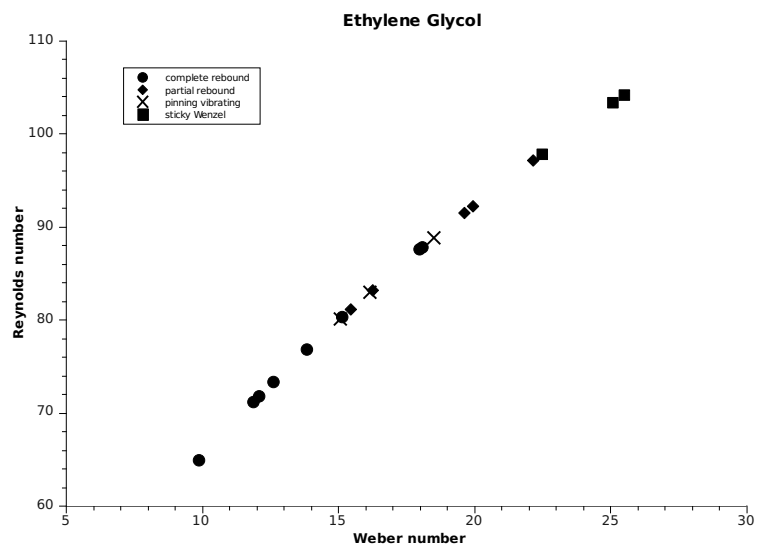


Figure 24: Sample 12. Falling heights ranging from 10.2 till 25.8 mm, impact speeds range from 0.45 till 0.71 m/s with a droplet diameter of  $2.1 \pm 0.1$  mm. Highest (partial) rebound was observed at 12.3 mm with an impact speed of 0.49 m/s.

## References

- [1] Purity of the sacred lotus, or escape from contamination in biological surfaces. *Planta*, 202(1):1–8, Apr. 1997.
- [2] Harrick Plasma; Plasma applications: Surface adhesion and wettability. [http://www.harrickplasma.com/applications\\_adhesion.php](http://www.harrickplasma.com/applications_adhesion.php), March 2012.
- [3] A. W. Adamson and A. P. Gast. *Physical chemistry of surfaces, 6th edition*. Wiley, New York, 1997.
- [4] A. Alizadeh, V. Bahadur, S. Zhong, W. Shang, R. Li, J. Ruud, M. Yamada, L. Ge, A. Dhinojwala, and M. Sohal. Temperature dependent droplet impact dynamics on flat and textured surfaces. *Applied Physics Letters*, 100(11):111601, 2012.
- [5] S. Banerjee. Simple derivation of Young, Wenzel and Cassie-Baxter equations and its interpretations. *eprint arXiv*, 2008.
- [6] G. Barnes and I. Gentle. *Interfacial Science, An Introduction*. Oxford University Press, 1st edition, 2005.
- [7] A. B. D. Cassie and S. Baxter. Wettability of porous surfaces. *Transactions of the Faraday Society*, 1944.
- [8] L. Chen, Z. Xiao, P. C. H. Chan, Y.-K. Lee, and Z. Li. A comparative study of droplet impact dynamics on a dual-scaled superhydrophobic surface and lotus leaf. *Applied Surface Science*, 257:8857–8863, Aug. 2011.
- [9] D. Debuissou, R. Dufour, V. Senez, and S. Arscott. Wetting on smooth micropatterned defects. *Applied Physics Letters*, 99(18):184101, 2011.
- [10] C. W. Extrand. Modeling of ultralyophobicity: suspension of liquid drops by a single asperity. *Langmuir*, 21(23):10370–10374, 2005. PMID: 16262294.
- [11] L. Gao and T. J. McCarthy. Contact angle hysteresis explained. *Langmuir The ACS Journal Of Surface And Colloids*, 22(14):6234–6237, 2006.
- [12] W. M. Haynes, editor. *CRC Handbook of Chemistry and Physics*. CRC Press, 92 edition, 2011 - 2012.
- [13] J. N. Lee, C. Park, and G. M. Whitesides. Solvent compatibility of poly(dimethylsiloxane)-based microfluidic devices. *Analytical Chemistry*, 75(23):6544–6554, 2003.
- [14] S. E. Lee, K. W. Lee, J.-H. Kim, K.-C. Lee, S. S. Lee, and S. U. Hong. Mass-producible superhydrophobic surfaces. *Chem. Commun.*, 47:12005–12007, 2011.
- [15] F. M. Y. C. M. Reyssat, A. Pepin and D. Quere. Bouncing transitions on micro-textured materials. *EUROPHYSICS LETTERS*, 74 (2):306–312, 2006.

- [16] A. Marchand, J. H. Weijs, J. H. Snoeijer, and B. Andreotti. Why is surface tension a force parallel to the interface? *American Journal of Physics*, 79(10):999–1008, 2011.
- [17] A. Mata, A. Fleischman, and S. Roy. Characterization of polydimethylsiloxane (pdms) properties for biomedical micro/nanosystems. *Biomedical Microdevices*, 7:281–293, 2005. 10.1007/s10544-005-6070-2.
- [18] J. C. McDonald, D. C. Duffy, J. R. Anderson, D. T. Chiu, H. Wu, O. J. A. Schueller, and G. M. Whitesides. Fabrication of microfluidic systems in poly(dimethylsiloxane). *ELECTROPHORESIS*, 21(1):27–40, 2000.
- [19] A. Merlen and P. Brunet. Impact of drops on non-wetting biomimetic surfaces. *Journal of Bionic Engineering*, 6(4):330–334, Dec. 2009.
- [20] C. NEINHUIS and W. BARTHLOTT. Characterization and distribution of water-repellent, self-cleaning plant surfaces. *Annals of Botany*, 79(6):667–677, 1997.
- [21] M. Nosonovsky. Multiscale roughness and stability of superhydrophobic biomimetic interfaces. *Langmuir*, 23(6):3157–3161, 2007.
- [22] A. Savitzky and M. J. E. Golay. Smoothing and differentiation of data by simplified least squares procedures. *Analytical Chemistry*, 36(8):1627–1639, 1964.
- [23] E. S. Savoy and F. A. Escobedo. Molecular simulations of wetting of a rough surface by an oily fluid: Effect of topology, chemistry, and droplet size on wetting transition rates. *Langmuir*, 28(7):3412–3419, 2012.
- [24] P. Tsai, S. Pacheco, C. Pirat, L. Lefferts, and D. Lohse. Drop impact upon micro- and nanostructured superhydrophobic surfaces. *Langmuir*, 25(20):12293–12298, 2009. PMID: 19821629.
- [25] A. Tuteja, W. Choi, M. Ma, J. M. Mabry, S. A. Mazzella, G. C. Rutledge, G. H. McKinley, and R. E. Cohen. Designing superoleophobic surfaces. *Science*, 318(5856):1618–1622, 2007.
- [26] A. Tuteja, W. Choi, J. M. Mabry, G. H. McKinley, and R. E. Cohen. Robust omniphobic surfaces. *Proceedings of the National Academy of Sciences*, 2008.
- [27] R. N. Wenzel. Resistance of solid surfaces to wetting by water. *Industrial & Engineering Chemistry*, 28(8):988–994, 1936.
- [28] L. Xu, W. W. Zhang, and S. R. Nagel. Drop splashing on a dry smooth surface. *Phys. Rev. Lett.*, 94:184505, May 2005.
- [29] T. Young. An essay on the cohesion of fluids. *Philosophical Transactions of the Royal Society of London*, 95:65–87, 1805.

- [30] H. Zhao, K.-Y. Law, and V. Sambhy. Fabrication, surface properties, and origin of superoleophobicity for a model textured surface. *Langmuir*, 27(10):5927–5935, 2011.